Electron-positron momentum distributions associated with isolated silicon vacancies in 3*C*-SiC

A. Kawasuso*
Advanced Science Research Center, Japan Atomic Energy Research Institute, Watanuki, 1233, Takasaki, Gunma 370-1292, Japan

M. Yoshikawa and H. Itoh
Takasaki Establishment, Japan Atomic Energy Research Institute, Watanuki, 1233, Takasaki, Gunma 370-1292, Japan

T. Chiba
National Institute for Materials Science, Namiki, 1-1, Tsukuba 305-0044, Japan

T. Higuchi and K. Betsuyaku
Mizuho Information and Research Institute, 2-3, Kanda, Nishikicho, Chiyoda-ku, Tokyo 101-8843, Japan

F. Redmann and R. Krause-Rehberg
Martin-Luther Universität, Halle-Wittenberg, FB Physik, Friedemann-Bach-Platz 6, D-06108, Halle, Germany
(Received 15 December 2004; revised manuscript received 15 March 2005; published 8 July 2005)

Two-dimensional angular correlation of annihilation radiation (2D-ACAR) and coincidence Doppler broadening (CDB) of annihilation radiation measurements have been performed on electron-irradiated *n*-type 3*C* -SiC in which isolated silicon vacancies are responsible for positron trapping. After irradiation, the intensity of the CDB spectrum increased and decreased in low- and high-momentum regions, respectively. These features were explained by a theoretical calculation considering silicon vacancies. The central region of the 2D-ACAR spectra became isotropic after iradiation, while the overall anisotropies extending within the Jones zone were conserved suggesting that isolated silicon vacancies have tetrahedral symmetry, as expected from a previous electron spin resonance study.

DOI: 10.1103/PhysRevB.72.045204 PACS number(s): 61.72.Ji, 61.72.Cc, 61.72.Bb, 61.80.Fe

I. INTRODUCTION

Extensive studies have been carried out to characterize point defects in SiC that are induced by irradiation because of their significant influence on electrical and optical properties. In contrast to the complexity of hexagonal polytype, 3*C*-SiC exhibits a rather simple outlook. 3*C*-SiC holds the cubic (zinc-blende) structure with three bilayers in the unit cell.[1] Hence, there are no intrinsic stacking faults in ideal 3*C*-SiC, unlike the case of hexagonal SiC. In early electron spin resonance (ESR) studies on electron-irradiated 3*C*-SiC, both isolated silicon and carbon vacancies are identified. Isolated silicon vacancies induced by electron irradiation are thermally annealed below 1000 °C via two decays.[2] Isolated carbon vacancies are annealed out below 500 °C.[3] Electrical measurements also show that the reduced carrier concentration due to irradiation is recovered by annealing below 1000 °C.[4–6]

Silicon vacancies in 3*C*-SiC are responsible for positron trapping and give rise to a prolonged annihilation lifetime and increased peak intensity (called the *S* parameter) of the Doppler broadening spectrum of annihilation radiation. It was confirmed that the annealing behavior of the positron lifetime and *S* parameter is consistent with that of the ESR signal intensity related to negatively charged silicon vacancies.[7,8] After the disappearance of silicon vacancies, no positron trapping centers have been confirmed, although a transformation mechanism of silicon vacancies to complexes composed of carbon vacancies and carbon antisites is proposed by theoretical considerations.[9,10] No positron trapping due to carbon vacancies in 3*C*-SiC has been observed. In comparison to silicon vacancies, carbon vacancies may act as very weak positron trapping centers. In fact, the theoretical positron lifetime for carbon vacancies is only 5–7 ps greater than bulk lifetime.[11,12] Thus, it appears that the detection of carbon vacancies is problematic, especially when they coexist with silicon vacancies. Although carbon vacancies are considered to be detectable when only carbon atoms are displaced by low energy electron irradiation,[13,14] careful studies are still required to justify this assertion.[15,16]

In this study, we carried out both coincidence Doppler broadening (CDB) and two-dimensional angular correlation of annihilation radiation (2D-ACAR) measurements on *n*-type 3*C*-SiC irradiated with fast electrons in which negatively charged silicon vacancies are the major positron trapping centers. These techniques are capable of characterizing defects in semiconductors.[17–20] The CDB method is able to demonstrate electron momentum distributions spectroscopically in a wide range.[21,22] In some cases, the examination of high-momentum region revealed the chemical environments of positron annihilation sites. From 2D-ACAR spectra, the anisotropies of electron-momentum distributions, which are closely related to the crystal bonding and geometrical symmetry of defects, can be extracted.[23] Although positron lifetime is easy to understand because it is a single parameter denoting the size of a vacant site, the momentum measurements provide more dimensional and electronic information. We will show that the CDB and 2D-ACAR spectra for 3*C*-SiC after electron irradiation are explained considering isolated silicon vacancies having tetrahedral symmetry.

II. EXPERIMENT

Specimens used in this study were chemical-vapor-deposition (CVD) grown *n*-type 3*C*-SiC(001) crystals with thicknesses of 18 and 154 μm on Si(001) substrates. The 18-μm-thick crystals were grown by us. The 154-μm-thick crystals (separated from the Si substrate) were supplied by Dr. Nagasawa of Hoya Advanced Semiconductor Technologies Co., Ltd. The qualities of these crystals were inspected by electron and x-ray diffraction techniques. No mosaic structures were observed. Both crystals were doped with nitrogen and the carrier densities were approximately 1×10^{16} cm^{-3}. The dislocation densities were below 10^4 cm^{-2}. In the as-grown state, the vacancy concentrations were under the detection limit of positron annihilation ($<10^{15}$ cm^{-3}). To introduce silicon vacancies, these specimens were subjected to electron irradiation. The thinner specimens were irradiated with 2 MeV electrons to a dose of $3\times10^{17}e$ cm^{-2} using a Dynamitron accelerator and the thicker specimens with 1 MeV electrons to a dose of $6\times10^{17}e$ cm^{-2} using a Cockcroft-Walton accelerator keeping the temperature below 40 °C. After irradiation, the positron lifetime and Doppler broadening *S* parameter showed comparable annealing behavior to that of the ESR signal intensity related to negatively charged silicon vacancies.[7]

Monoenergetic positrons with an energy of 30 keV were implanted into the thinner specimens and annihilation gamma rays were detected by two Ge detectors connected to the FAST-ComTec MPA-Win device.[24] Detecting coincidence events, CDB spectra were obtained at room temperature. In each spectrum, 4×10^7 counts were accumulated. The energy resolution was approximately 1 keV in full width at half maximum (FWHM). Here, the Doppler energy shift of 1 keV corresponds to 3.92 mrad in angle deviation from π of two annihilation radiations and 0.54 a.u. in momentum shift. A positron source (^{22}NaCl) with an activity of 0.37 MBq deposited on a titanium thin film was sandwiched with the thicker specimens and positron lifetime measurements were conducted at room temperature. The time resolution of the spectrometer was 200 ps in FWHM. More than 3×10^6 counts were accumulated in one spectrum. To avoid the transmission of fast positrons through the specimens, three layers of specimens (154 μm$\times$3) were stacked on both sides of the source. The obtained positron lifetime spectra were analyzed by one or two exponential decay components [$L(t)=(I_1/\tau_1)\exp(-t/\tau_1)+(I_2/\tau_2)\exp(-t/\tau_2)$, where $I_{1,2}$ are the intensities and $\tau_{1,2}$ are the lifetimes] after resolution deconvolution and source correction using the PATFIT program.[25] Positrons emitted from a source with an activity of 0.84 GBq were also implanted into the thicker specimens from the $[00\bar{1}]$ direction and annihilation gamma rays were detected by two position- sensitive Anger cameras placed 7 m away from the specimen.[23] Detecting coincidence events, 2D-ACAR spectra, $N(p_x,p_y)$, were obtained at room temperature. In each spectrum, more than 5×10^7 counts were accumulated. Here, p_x and p_y are the horizontal and vertical axes, respectively, on the detector plane and p_z is the normal axis to it. The [001] direction is always parallel to the p_y axis. By rotating the specimens around the [001], the [100] or [110] (the [010] or $[\bar{1}10]$) direction paralleled to the p_x (p_z) axis. The geometrical resolutions along the p_x and p_y axes were 1.0 mrad and 0.5 mrad, respectively. To observe the detailed topological features of ACAR spectrum, the following anisotropy plot was made.

$$A(p_x,p_y)=N(p_x,p_y)-\frac{1}{2\pi}\int_0^{2\pi}N(p,\theta)d\theta, \tag{1}$$

where $p^2=p_x^2+p_y^2$ and $\theta=\arctan(p_y/p_x)$. Considering the symmetry of cubic crystal, the obtained spectra were averaged by the folding treatment. In the [100]-[001] projection, the spectra were folded around the [010] axis keeping a fourfold symmetry. In the [110]-[001] projection, the spectra were folded around the $[\bar{1}10]$ keeping a twofold symmetry.

III. CALCULATION

To interpret the experimental results in detail, the Doppler broadening and 2D-ACAR spectra were computed within the local density approximation.[26] The valence electron momentum distribution was calculated using the conventional scheme

$$\rho_v(\mathbf{p})=\pi r_e c^2\sum_n\left|\int e^{-i\mathbf{pr}}\Psi_+(\mathbf{r})\Psi_n(\mathbf{r})\sqrt{\gamma(\mathbf{r})}d\mathbf{r}\right|^2, \tag{2}$$

where r_e is the classical electron radius, c is the speed of light, $\Psi_+(\mathbf{r})$ is the positron wave function, $\Psi_n(\mathbf{r})$ is the valence electron wave function of the nth band, and $\gamma(\mathbf{r})$ is the enhancement factor. The summation was performed over all the occupied states. The core electron momentum distribution was calculated following Alatalo's method[21]

$$\rho_c(\mathbf{p})=\pi r_e c^2\sum_{i,nlm}\left|\int e^{-i\mathbf{pr}}\Psi_+(\mathbf{r})\Psi_{i,nlm}(\mathbf{r}-\mathbf{R}_i)\sqrt{\gamma(\mathbf{r})}d\mathbf{r}\right|^2, \tag{3}$$

where $\Psi_{i,nlm}(\mathbf{r}-\mathbf{R}_i)$ represents the core electron wave function specified by the principal, azimuthal, and magnetic quantum numbers (nlm) for the ith atom and $\mathbf{R}_i$ denotes the position vector. The total momentum distribution is given by $\rho(\mathbf{p})=\rho_v(\mathbf{p})+\rho_c(\mathbf{p})$. A supercell including 108 Si and 108 C atoms ($3\times3\times3$ conventional unit cells) was constructed for the perfect lattice. The lattice constant was fixed to be 4.37 Å.[27] The valence electron wave function was calculated based on the norm-conserving pseudopotential method considering the Γ point using the ABINIT 4.1.4 code.[28] The cutoff energy of the plane wave basis set was typically 60 Ry. The core electron wave function was represented by the Slater function parametrized by Clementi and Roetti to mimic the results of the Hartree-Fock calculation.[29] By considering the correlation interaction between a positron and electrons and the Coulomb interaction from ion cores, a self-consistent positron wave function was calculated based on the two-component density functional theory in order to minimize the energy functional.[30] The Boroński-Nieminen enhancement factor was adopted.[30] In the calculation of vacancies, relevant atoms were removed from the perfect lattice. The

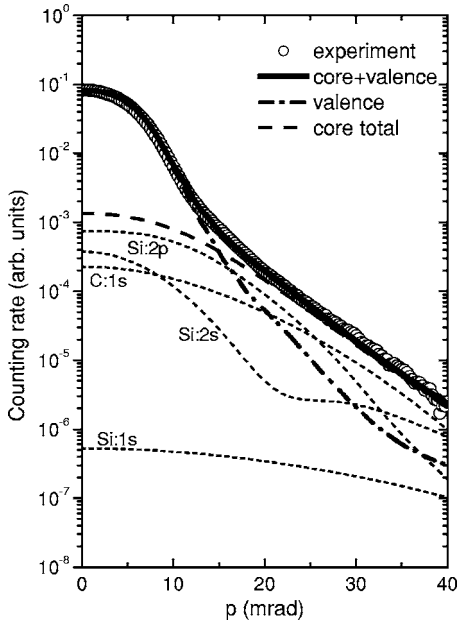

FIG. 1. Experimental CDB spectrum from as-grown 3*C*-SiC of 18 μm thickness (open circles) and theoretical curve (solid line). The theoretical curve consists of contributions from valence electrons (chained line) and core electrons (dashed line). The core contribution is further decomposed into individual inner shell orbitals (short dashed lines).

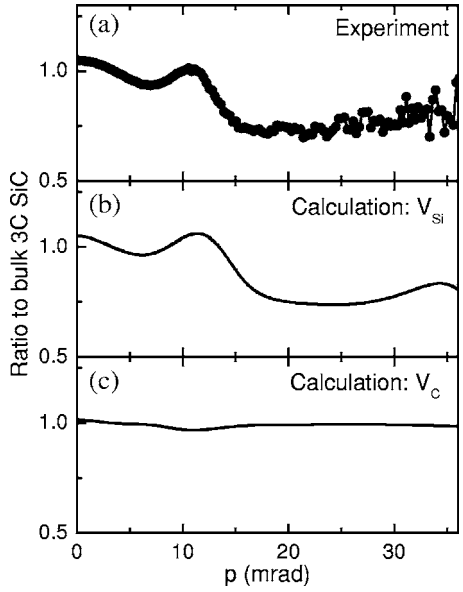

FIG. 2. CDB curves (ratio to bulk 3*C*-SiC spectrum) obtained from (a) 3*C*-SiC (18 μm thick) irradiated with 2 MeV electrons to a dose of $3\times10^{17}e$ cm^{-2}, (b) calculation for an isolated silicon vacancy, and (c) calculation for an isolated carbon vacancy.

forces acting on the atoms were not considered in the calculation because of the limitation of our computer, while the effects of lattice relaxation on the positron annihilation characteristics were examined by shifting the nearest-neighbor atoms around vacancies. 2D- and 1D-ACAR spectra were subsequently obtained by integrating $\rho(\mathbf{p})$ in one (p_z) and two (p_y,p_z) momentum axes, respectively. The Doppler broadening spectra were obtained by convoluting 1D-ACAR spectra with the Gaussian resolution function of measurement system. Here we assumed the FWHM of the Gaussian function to be 4 mrad. The positron annihilation rate (inverse of lifetime) was obtained by integrating the momentum density in all momentum space. The positron lifetimes for a perfect 3*C*-SiC lattice, an unrelaxed carbon vacancy, an unrelaxed silicon vacancy, and a silicon vacancy with 10% outward relaxation of the nearest-neighbor atoms were 136 ps, 138 ps, 171 ps, and 192 ps, respectively. These are in good agreement with those reported in the previous researches,[11,12] suggesting the validity of the calculation.

IV. RESULTS AND DISCUSSION

Figure 1 shows the CDB spectrum obtained from the as-grown thinner specimens (18 μm thick) and its comparison with the calculated one. The measured spectrum is well reproduced by the calculation. This confirms the validity of the calculation. Figure 2(a) shows the ratio curve of CDB spectra between 2 MeV-electron-irradiated and as-grown states [$N_{ir}(p)/N_{ag}(p)$, where the subscripts "*ir*" and "*ag*" denote "irradiated" and "as-grown," respectively]. The intensity in the low-momentum region ($p<10$ mrad) is greater than unity and that in the high-momentum region ($p>15$ mrad) is less than unity. These represent a reduction in the core annihilation rate and hence relative increase of the valence annihilation rate because of the annihilation of positrons at vacancy defects. The peak at $p=11-12$ mrad is explained as the disappearance of the dip at the Jones zone in the irradiated state because of the lack of translational symmetry due to vacancies. Figures 2(b) and 2(c) show the CDB ratio curves calculated for an isolated silicon vacancy and a carbon vacancy, respectively. It is found that the curve for a silicon vacancy is compatible with the experiment [Fig. 2(a)], but that for a carbon vacancy is not. This confirms that isolated silicon vacancies are responsible for positron trapping. The *S* and *W* parameters obtained from the present calculation are 1.032 and 0.802, respectively, relative to the bulk values (the windows for the *S* and *W* parameters are 0–3 mrad and 15–25 mrad, respectively). These are also consistent with experimentally obtained values for silicon vacancies in 3*C*-SiC.[7,31]

As seen in Fig. 2(c), the calculated CDB ratio curve for a carbon vacancy is rather flat. Hence, the *S* parameter for carbon vacancies is very similar to that for the bulk value. This result is also in agreement with the previous report that carbon vacancies are practically invisible in the Doppler broadening measurement.[32] In the present experiment, both silicon vacancies and carbon vacancies should be created by irradiation because the electron energies are high enough to displace both carbon and silicon atoms. However, the presence of carbon vacancies is concealed by the strong influence of silicon vacancies due to the above reasons. This situation is similar to the case of positron lifetime experiment reported previously.[8]

In a previous positron study,[13] a CDB ratio curve obtained after 300 keV electron irradiation is attributed to carbon vacancies because the curve shape in the high-momentum re-

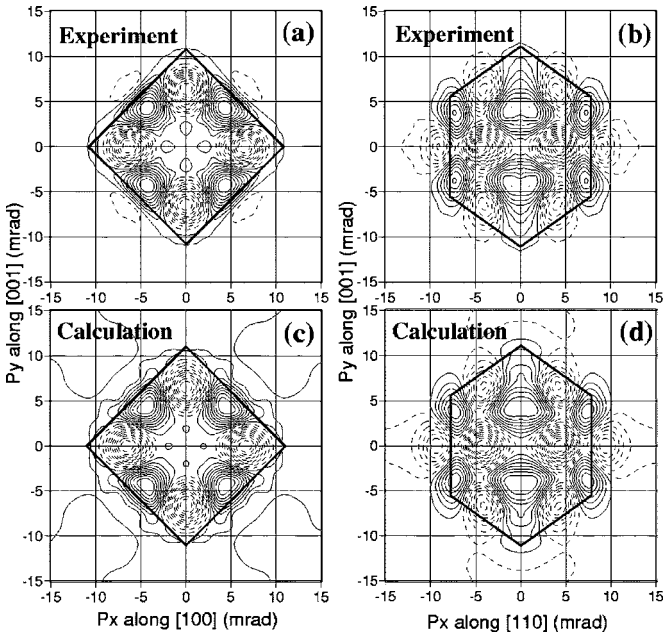

FIG. 3. Experimental 2D-ACAR anisotropy spectra for the as-grown 3*C*-SiC (154 μm thick) at (a) the [100]-[001] projection and (b) the [110]-[001] projection. Theoretical 2D-ACAR anisotropy spectra for the perfect 3*C*-SiC lattice at (c) the [100]-[001] projection and (d) the [110]-[001] projection. Solid and dashed lines represent positive and negative values, respectively. The contour spacing is 5% of the difference between the maximum and minimum intensities. Bold solid lines represent the area of the Jones zones.

gion appears to be different from that in the case of higher bombardment energy in which silicon vacancies are the predominant positron trapping centers. However, on the contrary, Steeds *et al.*[33] demonstrated that the threshold energy for the silicon displacement lies below 250 keV. This implies a possibility that silicon vacancies are observed instead of carbon vacancies in Ref. 13. The overall shape of the CDB ratio curve in Ref. 13 is indeed different from the curve (c) for a carbon vacancy but similar to the curve (b) for a silicon vacancy in Fig. 2. The above contradictions should be clarified in the future.

Figures 3(a) and 3(b) show the 2D-ACAR anisotropy spectra at the [100]-[001] and [110]-[001] projections obtained from the as-grown thicker specimen (154 μm thick). In the former projection, a fourfold symmetry around the [010] axis is observed. In the latter projection, a twofold symmetry around the $[\bar{1}10]$ axis is observed. These well represent the feature of tetrahedral crystal bonding.[23] Figures 3(a) and 3(b) also show that the major part of the momentum density is accommodated within the Jones zone.[34] These observations are common in semiconductors having diamond and zinc-blende structures. Figures 3(c) and 3(d) show the 2D-ACAR anisotropy spectra calculated theoretically. The experimental spectra are in fact well reproduced. The cross-sectional 2D-ACAR spectra were also found to agree with the calculation.

After 1-MeV electron irradiation, the central intensities of 2D-ACAR spectra were found to increase in a similar manner as Doppler broadening spectra. The positron lifetime spectrum was well approximated using two exponential decay components: $\tau_1=98\pm8$ ps and $\tau_2=199\pm1$ ps with the intensities of $I_1=27\pm1\%$ and $I_2=73\pm1\%$, respectively. The second lifetime is attributed to the annihilation of positrons at silicon vacancies.[8] In the as-grown state, only one lifetime of $\tau=142\pm1$ ps, which agrees with the bulk lifetime (τ_B),[7] was obtained. The bulk lifetime (156 ps) expected from the above lifetimes and intensities, however, exceeds it. The positron trapping rate is estimated to be $\kappa=(1/\tau_B-1/\tau_2)I_2/I_1=5.4$ ns^{-1} without τ_1. From the two-state trapping model,[35] the first lifetime should be 80 ps$[=(1/\tau_B+\kappa)^{-1}]$. This is also lower than the experimental value (98±8 ps). The above discrepancies are simply due to the uncertainty of τ_1 in the decomposition procedure because of the limited time resolution. Positrons annihilate both at the bulk and the silicon vacancies. Indeed, the previous studies showed that the annealing behavior of the trapping rate is consistent with that of the ESR T_1 signal arising from silicon vacancies.[7,8] Also the possiblity of divacancies is ruled out although the above lifetime is close to that for divacancies.[36] The vacancy-trapped fraction is estimated to be 0.43 $[=\kappa/(1/\tau_B+\kappa)]$. Consequently, the ACAR spectra for silicon vacancies were obtained by subtracting the bulk components from the original spectra, i.e., $N_{ir}(p_x,p_y)-(1-f)N_{ag}(p_x,p_y)$, where f denotes the vacancy-trapped fraction. Figures 4(a) and 4(b) show the 2D-ACAR anisotropy spectra for silicon vacancies. From Fig. 4(a) it is found that the fourfold symmetry in the low-momentum region ($p<3$ mrad) observed for the as-grown state disappears after irradiation. That is, the momentum distribution becomes more isotropic near the central region. This corresponds to the destruction of the translational symmetry. However, the overall topological features inside the Jones zone are maintained even after irradiation. That is, the [100]-[001] projection shows the fourfold rotational symmetry around the [010] axis and the pronounced anisotropy along the [101] and $[\bar{1}01]$ axes. The [110]-[001] projection shows the twofold rotational symmetry around the $[\bar{1}10]$ axis. Different anisotropies at different projections reflect the geometrical symmetry of vacancies. These anisotropies are explicitly interpreted in terms of the tetrahedral bonding. Actually, the above observations are in good agreement with the theoretical 2D-ACAR anisotropy spectra calculated for an isolated silicon vacancy, as shown in Figs. 4(c) and 4(d). It was also confirmed that the breathing-mode lattice relaxation around the vacancy has a minor role.

Coulson and Larkins employed the linear combination of atomic orbital (LCAO) scheme for describing possible electronic transitions associated with single vacancies in diamond, which have tetrahedral symmetry.[37] Based on this analogy, one-electron orbitals can be given by $\phi_1+\phi_2+\phi_3+\phi_4$ for the A_1 state, $\phi_1-\phi_2-\phi_3+\phi_4$, $\phi_1+\phi_2-\phi_3-\phi_4$, and $\phi_1-\phi_2+\phi_3-\phi_4$ for the T_2 state, where $\phi_i(i=1-4)$ represents the sp^3 hybridized orbitals of the four nearest-neighbor carbon atoms around a silicon vacancy. Thus, the upper T_2 state is threefold degenerated, i.e., a high spin state.[38] The calculated 2D-ACAR anisotropies in Figs. 4(c) and 4(d) mostly reflect the nature of the A_1 state and the T_2 state appears to play only a minor role. The ACAR spectra of vacancies having tetrahedral symmetry have been studied in detail by Saito

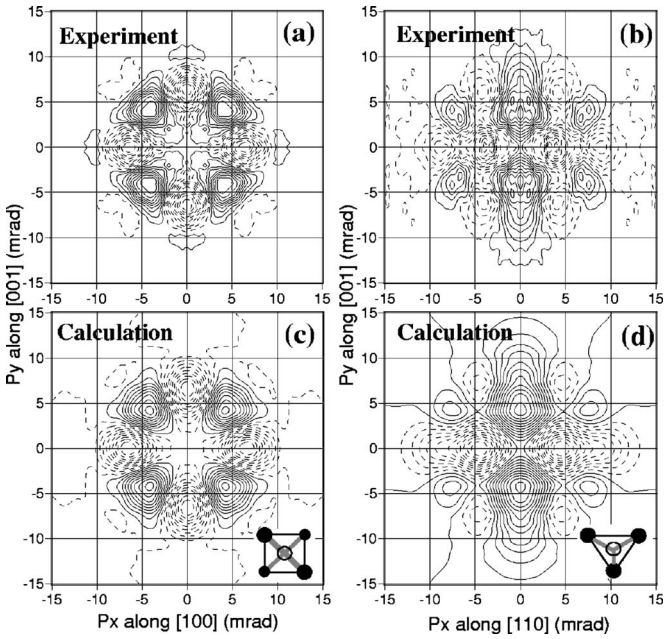

FIG. 4. Experimental 2D-ACAR anisotropy spectra for 3*C*-SiC (154 μm thick) irradiated with 1 MeV electrons to a dose of $6\times10^{17}e$ cm^{-2} at (a) the [100]-[010] projection and (b) the [110]-[001] projection. Here, the bulk components are subtracted from the original spectra as described in the text. Theoretical 2D-ACAR anisotropy spectra for an isolated silicon vacancy in 3*C* -SiC lattice at (c) the [100]-[010] projection and (d) the [110]-[001] projection. Solid and dashed lines represent positive and negative values, respectively. The contour spacing is 5% of the difference between the maximum and minimum intensities. Atomic arrangements around silicon vacancies observed from the $[0\bar{1}0]$ and $[1\bar{1}0]$ directions are schematically drawn in (c) and (d), respectively.

et al.[39] Their results show that the ACAR spectrum is mainly determined by the totally symmetric state, i.e., the A_1 state. Similar results were reported for vacancies in GaAs by McMullen *et al.*[40] In Fig. 4(c), the peaks along the [101] and $[\bar{1}01]$ axes are due to the projection of the dangling bond along the [111], $[\bar{1}1\bar{1}]$, $[\bar{1}\bar{1}1]$, and $[1\bar{1}\bar{1}]$ axes. In Fig. 4(d), the observed peaks are explained as an overlapping of the projections of momentum distributions associated with the dangling bonds. Thus, the ACAR spectra are consistent with the fact that positrons annihilate at isolated silicon vacancies with tetrahedral symmetry.

V. CONCLUSION

In conclusion, we have studied silicon vacancies in 3*C*-SiC introduced by electron irradiation using CDB and 2D-ACAR techniques. It was found that the intensity of the CDB spectrum increased and decreased in low- and high-momentum regions, respectively, when silicon vacancies were present. The CDB ratio curve was reproduced by theoretical calculation considering silicon vacancies but not carbon vacancies. Although the anisotropy of the 2D-ACAR spectrum in a low-momentum region diminished after irradiation, the overall anisotropies were conserved. This feature was well explained considering silicon vacancies with tetrahedral symmetry.

ACKNOWLEDGMENTS

We thank Dr. Nagasawa of Hoya Advanced Semiconductor Technologies Co., Ltd. for providing us with thick 3*C*-SiC crystals. This work was partly supported by the Alexander von Humboldt Foundation and by the Nuclear Energy Fundamentals Crossover Research in the Ministry of Education, Culture, Sports, Science, and Technology (MEXT), Japan. In the positron calculation, we used some resources developed in "Embedded High-Performance Computing (EHPC) Project" supported by Special Coordination Funds for Promoting Science and Technology of MEXT, Japan.

*Corresponding author. Electronic address: ak@taka.jaeri.go.jp

[1] F. Bechstedt, P. Käckell, A. Zywietz, K. Karch, B. Adolph, K. Tenelsen, and J. Furthmüller, Phys. Status Solidi B **202**, 35 (1997).

[2] H. Itoh, N. Hayakawa, I. Nashiyama, and E. Sakuma, J. Appl. Phys. **66**, 4529 (1989).

[3] H. Itoh, M. Yoshikawa, I. Nashiyama, S. Misawa, H. Okumura, and S. Yoshida, J. Electron. Mater. **21**, 707 (1992).

[4] H. Itoh, M. Yoshikawa, I. Nashiyama, S. Misawa, H. Okumura, and S. Yoshida, in *Amorphous and Crystalline Silicon Carbide III*, edited by G. L. Harris, M. G. Speneer and C. Y. Yang (Springer-Verlag, Berlin, 1992), p. 143.

[5] N. Nagesh, J. W. Farmer, R. F. Davis, and H. S. Kong, Appl. Phys. Lett. **50**, 1138 (1990).

[6] N. Nagesh, J. W. Farmer, R. F. Davis, and H. S. Kong, Radiat. Eff. Defects Solids **112**, 77 (1990).

[7] A. Kawasuso, in *Silicon Carbide—Recent Major Advances*, edited by W. J. Choyke, H. Matsunami, and G. Pensl (Springer-Verlag, Berlin, 2004), p. 563.

[8] A. Kawasuso, H. Itoh, N. Morishita, M. Yoshikawa, T. Ohshima, I. Nashiyama, S. Okada, H. Okumura, and S. Yoshida, Appl. Phys. A **67**, 209 (1998).

[9] M. Bockstedte, A. Mattausch, and O. Pankratov, Phys. Rev. B **68**, 205201 (2003).

[10] E. Rauls, T. Linger, Z. Hajnal, S. G. Weber, T. Frauenheim, and J. M. Speath, Phys. Status Solidi B **217**, R1 (2000).

[11] G. Brauer, W. Anwand, E. M. Nicht, J. Kuriplach, M. Sŏb, N. Wagner, P. G. Coleman, M. J. Puska, and T. Korhonen, Phys. Rev. B **54**, 2512 (1996).

[12] T. E. M. Staab, L. M. Torpo, M. J. Puska, and R. M. Nieminen, Mater. Sci. Forum **353–356**, 533 (2001).

[13] A. A. Rempel, W. Sprengel, K. Blaurock, K. J. Reichle, J. Major, and H. E. Schaefer, Phys. Rev. Lett. **89**, 185501 (2002).

[14] X. D. Chen, C. L. Yang, M. Gong, W. K. Ge, S. Fung, C. D.

Beling, J. N. Wang, M. K. Lui, and C. C. Ling, Phys. Rev. Lett. **92**, 125504 (2004).
[15] J. Kuriplach, G. Brauer, W. Anwand, and W. Skorupa, Phys. Rev. Lett. **91**, 199601 (2003).
[16] J. W. Steeds, Phys. Rev. Lett. **91**, 109601 (2003).
[17] Z. Tang, M. Hasegawa, T. Chiba, M. Saito, A. Kawasuso, Z. Q. Li, R. T. Fu, T. Akahane, Y. Kawazoe, and S. Yamaguchi, Phys. Rev. Lett. **78**, 2236 (1997).
[18] R. Ambigapathy, C. Corbel, P. Hautojärvi, A. A. Manuel, and K. Saarinen, Appl. Phys. A **62**, 529 (1996).
[19] L. Gilgien, G. Galli, F. Gygi, and R. Car, Phys. Rev. Lett. **72**, 3214 (1994).
[20] M. Hakala, M. J. Puska, and R. M. Nieminen, Phys. Rev. B **57**, 7621 (1998).
[21] M. Alatalo, B. Barbiellini, M. Hakala, H. Kauppinen, T. Korhonen, M. J. Puska, K. Saarinen, P. Hautojärvi, and R. M. Nieminen, Phys. Rev. B **54**, 2397 (1996).
[22] P. Asoka-Kumar, M. Alatalo, V. J. Ghosh, A. C. Kruseman, B. Nielsen, and K. G. Lynn, Phys. Rev. Lett. **77**, 2097 (1996).
[23] Z. Tang, M. Hasegawa, T. Chiba, M. Saito, H. Sumiya, Y. Kawazoe, and S. Yamaguchi, Phys. Rev. B **57**, 12219 (1998).
[24] J. Gebauer, R. Krause-Rehberg, S. Eichler, and F. Böner, Appl. Surf. Sci. **149**, 110 (1999).
[25] P. Kirkegaard, N. Pederson, and M. Eldrup, PATFIT-88, Riso-M-2704 (1989).
[26] M. J. Puska and R. M. Nieminen, Rev. Mod. Phys. **66**, 841 (1994).
[27] A. Taylor and R. M. Jones, in *Silicon Carbide–A High Temperature Semiconductor* edited by J. R. O'Connor and J. Smiltens (Pergamon Press, New York, 1960), p. 147.
[28] X. Gonze *et al.*, Comput. Mater. Sci. **25**, 478 (2002).
[29] E. Clementi and C. Roetti, At. Data Nucl. Data Tables **14**, 177 (1974).
[30] E. Boroński and R. M. Nieminen, Phys. Rev. B **34**, 3820 (1986).
[31] H. Itoh, M. Yoshikawa, I. Nashiyama, L. Wei, S. Tanigawa, S. Misawa, H. Okumura, and S. Yoshida, Mater. Sci. Forum **117–118**, 501 (1993).
[32] S. Dannefaer, D. Craigen, and D. Kerr, Phys. Rev. B **51**, 1928 (1995).
[33] J. W. Steeds, F. Carosella, G. A. Evans, M. M. Ismail, L. R. Danks, and W. Voegeli, Mater. Sci. Forum **353–356**, 381 (2001).
[34] P. E. Mijnarends, Phys. Rev. B **4**, 2820 (1971).
[35] W. Brandt, in *Positron Annihilation*, edited by A. T. Stewart and L. O. Roelling (Academic Press, New York, 1967), p. 178.
[36] A. Polity, S. Huth, and M. Lausmann, Phys. Rev. B **59**, 10603 (1999).
[37] C. A. Coulson and F. P. Larkins, J. Phys. Chem. Solids **32**, 2245 (1971).
[38] L. Torpo, R. M. Nieminen, K. E. Laasonen, and S. Pöykkö, Appl. Phys. Lett. **74**, 221 (1999).
[39] M. Saito, A. Oshiyama, and S. Tanigawa, Phys. Rev. B **44**, 10601 (1991).
[40] T. McMullen and M. F. Bishop, Phys. Rev. B **55**, 4046 (1997).